The influence of Si on the primary protection of lean FeCrAl model alloys in O2 and O2+H2O at 600 °C: A microstructural investigation

Corrosion Science 179 (2021) 109155

Contents lists available at ScienceDirect

Corrosion Science

journal homepage: www.elsevier.com/locate/corsci

The influence of Si on the primary protection of lean FeCrAl model alloys in O_2 and O_2+H_2O at 600 °C—A microstructural investigation

V. Asokan *, J. Eklund, S. Bigdeli, T. Jonsson

Environmental Inorganic Chemistry, Department of Chemistry and Chemical Engineering, Chalmers University of Technology, S-412 96, Göteborg, Sweden

ARTICLE INFO

Keywords:
A. FeCrAl
A. Silicon
B. SEM
B. STEM
C. High temperature corrosion
C. Thermodynamic diagrams

ABSTRACT

The present study investigates the influence of Si on the high-temperature corrosion behavior of lean FeCrAl model alloys in O_2 and O_2+H_2O at 600 °C. The addition of Si prevented breakaway oxidation in O_2+H_2O which may be explained by the increased Al-content and reduced Cr-content in the oxide (O_2) as well as the Si-enrichment in the outer part of the scale (O_2+H_2O). A proposed explanation for the impact of Si-addition on the Cr- and Al-content was given by thermodynamic calculations which showed that the presence of Si increases the activity of Al in the alloy while reducing the activity of Cr.

1. Introduction

It is well known that FeCrAl alloys have the ability to form a protective α-alumina scale at high temperatures (900−1300 °C) [1–3]. In this temperature range the continuous scale of α-alumina acts as a strong diffusion barrier which protects the underlying metal from fast oxidation. Hence, FeCrAl alloys are considered an efficient corrosion resistant material in many high temperature applications, such as heating elements for various applications, including the electrical elements of gas burners, furnace rollers, ignitors, etc. Even though FeAl alloys may form α-alumina, addition of Cr has been shown to promote the formation of α-alumina, enabling FeCrAl alloys to formS this protective layer at lower Al-contents, thereby reducing the detrimental effect on the mechanical properties, caused by a high Al-content in the alloy. The mechanism behind this effect is known as the third element effect, i.e. the addition of a third element of a tertiary alloy system which can form an oxide with a stability intermediate to those of the two other elements [4]. By forming an initial chromia layer on the surface in the initial stage of the oxidation process, pO_2 under the scale is reduced which favors the formation of the more stable oxide (in this case α-alumina).

Recently, the oxidation behavior of FeCrAl alloys at medium high temperatures (500–700 °C) have been investigated [5–7]. In this temperature range, the formation of α-alumina occurs at such a low rate that transient forms of alumina are usually observed instead. In mild environments, e.g. in absence of water vapor and/or corrosive salt mixtures, the transient alumina layer may be protective enough to limit the propagation of the oxidation process [6,7]. However, the oxide microstructure of the thin protective scales is not well characterized.

Adding small amounts of Si to stainless steels (FeCr, FeCrNi) is known to improve the corrosion protection at high temperatures [8–18]. Si-containing alloys have been shown to form a SiO_2 layer at higher temperatures which may act as a diffusion barrier, protecting the alloy and inhibits the corrosion process. Even at lower temperatures (less than 500 °C), Si has been shown to contribute to an improved oxidation resistance. However, since the growth rate of SiO_2 is much slower at these temperatures, a very thin SiO_2 layer may be too thin to act as a diffusion barrier.

A recent study showed that minor additions of Si significantly influenced the corrosion behavior of lean FeCrAl alloys at 600 °C in environments with different degrees of corrosivity [6]. It was shown that the addition of Si could improve the properties of both the slow-growing alumina/chromia and the Fe-rich oxide (formed after breakaway). Because of the possibility to improve the protectiveness of both of these types of oxides, two new definitions were introduced, namely **primary** (chromia/alumina) and **secondary protection** (Fe-rich oxide) which corresponds to the oxides protecting the alloy before and after breakaway respectively. This approach is further described by Persdotter et al. [19]. The main focus of this study is to improve the understanding of the influence of Si on the primary protection of lean FeCrAl alloys.

Lean FeCrAl alloys with varying Si-content were exposed in an oxygen containing environment (in the absence of other corrosive species) which showed significant improvements on the primary protection upon

* Corresponding author.
E-mail address: vijayshankar.matsci@gmail.com (V. Asokan).

https://doi.org/10.1016/j.corsci.2020.109155
Received 22 June 2020; Received in revised form 16 November 2020; Accepted 19 November 2020
Available online 24 November 2020

the addition of Si [6]. With the absence of Si, the alloys formed iron oxide nodules as well as iron oxide formation on specific grains while this phenomenon did not occur with Si present in the alloy. However, very little is known about the mechanism behind this effect and the possible impact on the protective scale microstructure.

The addition of water vapor to an oxygen containing environment at high temperatures is known to accelerate the corrosion attack on chromia-forming alloys. This has been attributed to the vaporization of $CrO_2(OH)_2$ which leads to a continuous depletion of Cr and may eventually result in breakdown of the primary protection (chromia) [20] followed by a transition into the secondary regime (formation of faster growing Fe-rich oxide for Fe-based alloys). The oxidation rate of FeCrAl alloys at high temperatures (900 °C) has been shown to increase by the presence of water vapor even though breakdown did not occur [3]. It was suggested that the presence of water vapor stabilized the outward growing γ-alumina, inhibiting the transformation into α-alumina and resulted in a higher growth rate [2]. However, at lower temperatures (500 °C and 700 °C) the oxidation rate within the primary regime has been shown to be similar regardless of the presence of water vapor [21]. It is well known that transient alumina is formed at 600 °C, containing relatively high amounts of Cr (~10 at%) [5], which may result in a higher sensitivity to the presence of water vapor. A recent study showed that a marginal chromia/alumina former, a Fe10Cr4Al model alloy, lost the primary protection in the presence of water vapor at 600 °C, which resulted in the formation of fast-growing Fe-rich oxide [6]. However, upon addition of Si to the same type of alloy (Fe10Cr4Al2Si), the primary protection (alumina/chromia) could be retained in the same environment. The mechanism behind this effect is currently unknown and investigating the influence of Si-addition on the microstructure of the protective oxide is therefore of great interest.

The aim of the current work is to carry out a microstructural investigation of the scales formed on lean FeCrAl model alloys with and without Si in a dry (5 %O_2 + N_2(bal.)) and a wet (5 %O_2 + 20 % H_2O + N_2(bal.)) environment at 600 °C to increase the understanding regarding the mechanism(s) behind the effect of Si-addition on the primary protection of lean FeCrAl alloys. In addition, the oxide microstructure will be analyzed and compared with equilibrium calculations. The microstructure and kinetics will be connected to predict the oxidation mechanisms of lean FeCrAl alloys and the influence of Si additions at medium \high temperatures.

2. Experimental procedure

2.1. Sample preparation

Lean FeCrAl model alloys with two different compositions were used in this study, one without Si and the other with 2 wt% Si (overall composition of the alloys is shown in Table 1). Since the combination of high Al and Cr content in lean FeCrAl alloys has been shown to impair the mechanical properties of the material, lean FeCrAl model alloys were produced to investigate how these would withstand the present conditions in relation to more highly alloyed FeCrAl alloys in previous studies. Additionally, using lean FeCrAl model alloys simplifies the distinction of the influence of Si on the corrosion resistance of these materials since more highly alloyed FeCrAl alloys may be able to withstand the present environment regardless of the Si-content. Coupons with dimension of 10 × 12 mm with a hole of 1.5 mm in diameter were prepared by grinding (with SiC paper) and subsequent polishing (using 3 μm and 1 μm diamond suspensions) until a mirror-like surface was achieved.

Table 1
The nominal composition (wt%) of the model alloys.

Alloy name	Grain size	Cr	Al	Si	C	N	Zr
FeCrAl**0Si**	110–130 μm	10	4	0	0.025	0.015	0.29
FeCrAl**2Si**	110–130 μm	10	4	2	0.025	0.015	0.29

2.2. Exposure

Studied alloys were exposed at 600 °C in a horizontal silica tube furnace for up to 168 h in two different environments: 5 % O_2 + N_2(bal.) (dry O_2) and 5 % O_2 + 20 % H_2O + N_2(bal.) (wet O_2). Mass gain of exposed samples was recorded by weighing prior and after exposure. The gas flow was calibrated using a Bios Definer 220 M to achieve a total flow rate of 3 cm/s. The exposure procedure is described in more detail in [6].

Theoretical oxide thicknesses were calculated for the samples. The calculations are based on the assumption that the total mass gain originates from the density change due to the ingress of oxygen. Thus, the theoretical density change is given by Eq. (1):

$$\Delta\rho_{theoretical} = \rho_{M_xO_y} * \frac{M(O_2)}{M(M_xO_y)} \quad (1)$$

where $\rho_{M_xO_y}$ is the oxide density and $M(O_2)$ and $M(M_xO_y)$ is the molar mass of oxygen gas and the oxide respectively. Utilizing the definition of density:

$$\rho = \frac{m}{V} \quad (2)$$

where m is the mass gain (g/cm^2) and V is the volume of the oxide, Eqs. (1) and (2) can be combined:

$$V\ cm^3 = d\ cm * 1\ cm^2 = \frac{m}{\rho_{M_xO_y} * \frac{M(O_2)}{M(M_xO_y)}} \quad (3)$$

where d is the oxide thickness on an area of 1 cm^2. Hence, the oxide thickness in μm is given by Eq. (4):

$$d = \frac{m}{\rho_{M_xO_y} * \frac{m(O_2)}{m(M_xO_y)}} * 10000 \quad (4)$$

2.3. Analytical techniques

The surface morphology of the resulting oxides of the exposed samples were analyzed by means of scanning electron microscopy (SEM) (using secondary electrons (SE)) with an accelerating voltage of 5 kV using an Ultra55 by Zeiss Instruments. To characterize the oxidized regions in transmission electron microscopy (TEM), dual beam FIB (Focused Ion Beam)-SEM (FEI Versa 3D) was employed to lift out thin cross-sections from the exposed specimens. A protective platinum layer was deposited prior to the ion milling. The thin cross-sections were then lifted out and fixed onto a Cu TEM grid. The imaging/analysis of cross-sectional lift-out was done using an FEI Titan 80–300, operated at 300 kV in high angular annular dark field – scanning transmission electron microscopy (HAADF-STEM) mode with spot size 4 and an aperture size of 50 μm. Energy dispersive spectroscopy line scan analysis was performed in STEM to derive chemical quantifications through the oxide scale. Due to the technical difficulties in quantifying lighter elements, such as oxygen, only the concentrations of cations are considered.

2.4. Thermodynamic calculations

Thermodynamic equilibrium calculations were performed using Thermo-Calc software, version 2020a and database TCFE10 to be able to better interpret the experimental observations.

3. Results

3.1. Mass gain

Fig. 1a shows the mass gains of FeCrAl**0Si** and the FeCrAl**2Si** exposed in 5 %O_2 + N_2(bal.), and 5 % O_2 + 20 % H_2O + N_2(bal.) for 168 h. Only the FeCrAl**0Si** samples exposed in a wet environment shows a high mass gain indicating a non-protective scale. Fig. 1b displays the marked region in Fig. 1a with higher magnification in order to be able to detect the differences of the samples with low mass gains.

In the dry environment, both FeCrAl**0Si** and FeCrAl**2Si** exhibits low mass gains after 168 h exposure, see Fig. 1a and Table 2. This indicates the formation of a thin protective oxide scale. However, FeCrAl**2Si** displays a roughly 80 % lower mass gain than FeCrAl**0Si**, see Fig. 1b. A corresponding oxide thickness was calculated, based on the formation of Cr_2O_3/Al_2O_3 for all the samples with low mass gain. In the dry O_2 environment, the calculated thickness varies between 143/189 nm (using Cr_2O_3/Al_2O_3) for FeCrAl**0Si** and 32/42 nm (using Cr_2O_3/Al_2O_3) for FeCrAl**2Si**. In order to investigate the kinetics of the oxidation process for FeCrAl**0Si** (to determine if the higher mass gain is reached at an early stage of the exposure), one set of 24 h exposures were in addition performed in the dry environment. The mass gain was 0.01 mg/cm^2, i.e. as expected lower than after 168 h exposure (0.023 mg/cm^2). However, this mass gain value is still higher than for FeCrAl**2Si** after 168 h.

In the O_2/H_2O-containing environment, the FeCrAl**2Si** samples exhibit low mass gains, indicating the formation of a thin oxide scale in the nanometer range. The mass gains are lower than when exposed in the dry O_2 environment and corresponds to a theoretical oxide thickness of about 1 nm. However, it is well known that Cr may evaporate from the protective scale at 600 °C [20,22] giving an underestimation of the theoretical thickness. In addition, when exposing the FeCrAl**0Si** sample in the wet environment for 168 h it exhibits a large mass gain, indicating the loss of the primary protection, resulting in a transition into the secondary regime (breakaway oxidation). Evaporation of Cr is a well-known breakaway mechanism responsible for breaking down Cr-rich oxides. The oxide scale after breakaway has previously been reported to consist of an Fe-rich oxide scale [6]. Since the present paper is focused on the influence of Si on the primary protection, the FeCrAl**0Si** samples exposed in the wet environment will not be taken into further consideration.

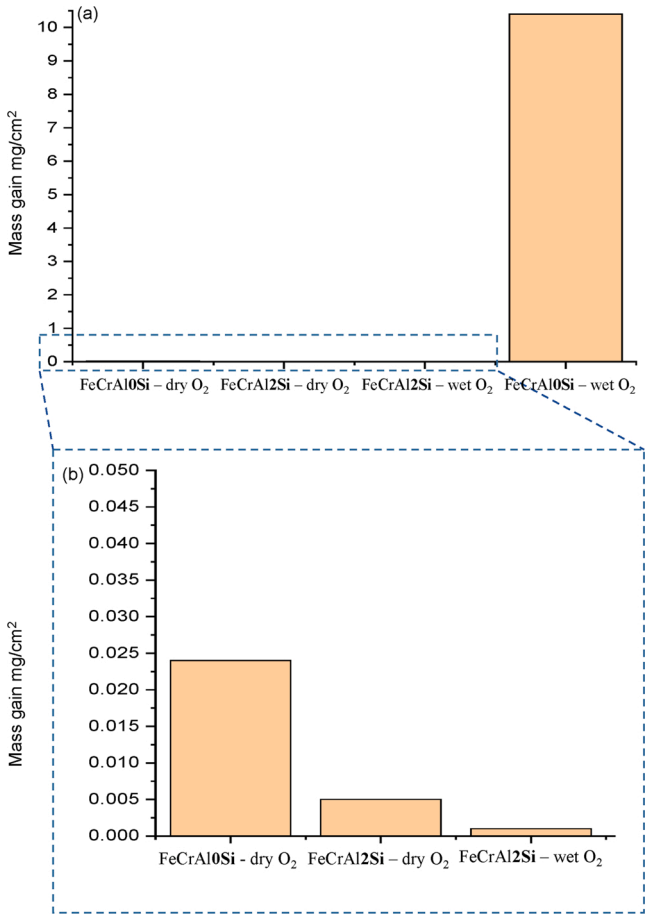

Fig. 1. Mass gains of FeCrAl0Si and FeCrAl2Si after exposure in dry O_2 (5 % O_2 + N_2 (bal.)) and wet O_2 (5 % O_2 + 20 % H_2O + N_2 (bal.)) at 600 °C for 168 h. Box in Fig. 1a is zoomed and displayed in Fig. 1b.

Table 2
Exposures of model alloys in different corrosive environments.

Sample	Exposure		Time (in hours)	Mass gain (mg/cm^2)
FeCrAl**0Si**	Dry	5 %O_2 + N_2(bal.)	24	0.01
FeCrAl**0Si**		5 %O_2 + N_2(bal.)	168	0.023
FeCrAl**2Si**		5 %O_2 + N_2(bal.)	168	0.005
FeCrAl**0Si**	Wet	5 %O_2 + 20% H_2O + N_2(bal.)	168	10.2
FeCrAl**2Si**		5 %O_2 + 20% H_2O + N_2(bal.)	168	0.001

3.2. Oxide microstructure and morphology

3.2.1. FeCrAl0Si – dry exposure

3.2.1.1. Surface morphology. Fig. 2 shows plan view SEM-SE images of the FeCrAl**0Si** after 24 h of exposure at 600 °C in 5 %O_2 + N_2 (bal.). The surface morphology of the sample indicates that about 60 % of the surface is covered by a thin base oxide (smooth areas) while approximately 40 % of the surface is covered by Fe-rich oxide islands. The shape of the Fe-rich oxide islands (which varies in size from 10−200 μm) indicates that specific grains have formed Fe-rich oxide while the rest remain fully protective. Small iron oxide particles (2−5 μm), originating from reactive elements (RE) particles, have formed and are evenly distributed on the surface.

Fig. 3(a–b) shows SEM-SE images of FeCrAl**0Si** exposed for 168 h at 600 °C in 5 %O_2 + N_2 (bal.). After 168 h exposure similar surface morphology features appear as after 24 h. However, the regions with Fe-rich oxide cover approximately 60 % of the surface after 168 h exposure. The amount of iron oxide particles did not increase with time when compared to 24 h exposure. The surface morphology of the Fe-rich oxide has in addition changed. Fig. 3b shows an Fe-rich oxide region in higher magnification. The surface morphology of Fe-rich regions in comparison with 24 h exposed sample looks different; for example, an additional growth is seen over already grown iron-oxide layers.

3.2.1.2. Oxide microstructure. The detailed microstructural investigation was focused on two of the three features observed on the surface morphology, i.e. the base oxide and the Fe-rich regions. Since the iron oxide nodules, associated with the RE-particles, did not change with time and cover only a small part of the surface, these were not further investigated by TEM. Ion-milled cross-sections of the base oxide and the Fe-rich regions were lifted out using the FIB/SEM and analyzed with TEM. The positions of the lift-outs are indicated in Fig. 3a.

Fig. 4 shows a STEM-HAADF image and a representative STEM-EDS line scan from the cross section of a grain covered with Fe-rich oxide on the FeCrAl**0Si** sample exposed at 600 °C in 5 %O_2 + N_2 (bal.) for 168 h. The HAADF image, displayed in Fig. 4a, shows that the oxide scale is 130−230 nm thick and consists of two different layers, distinguished by the difference in contrast (an upper layer in brighter contrast and a lower layer in darker contrast). Additionally, dark contrast streaks were

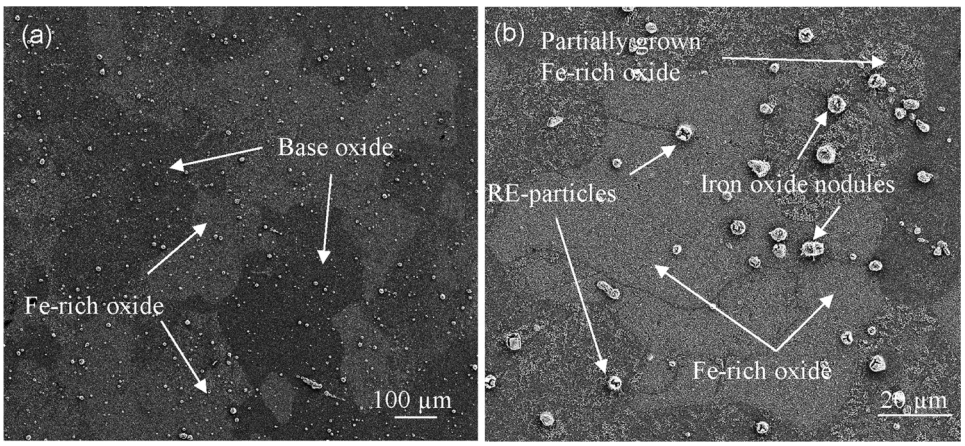

Fig. 2. (a–b) SEM-SE images at different magnifications of FeCrAl**0Si** after exposure in dry O_2 (5 % O_2 + N_2 (bal.)) at 600 °C for 24 h. Fig. 2b displays the key features in higher magnification.

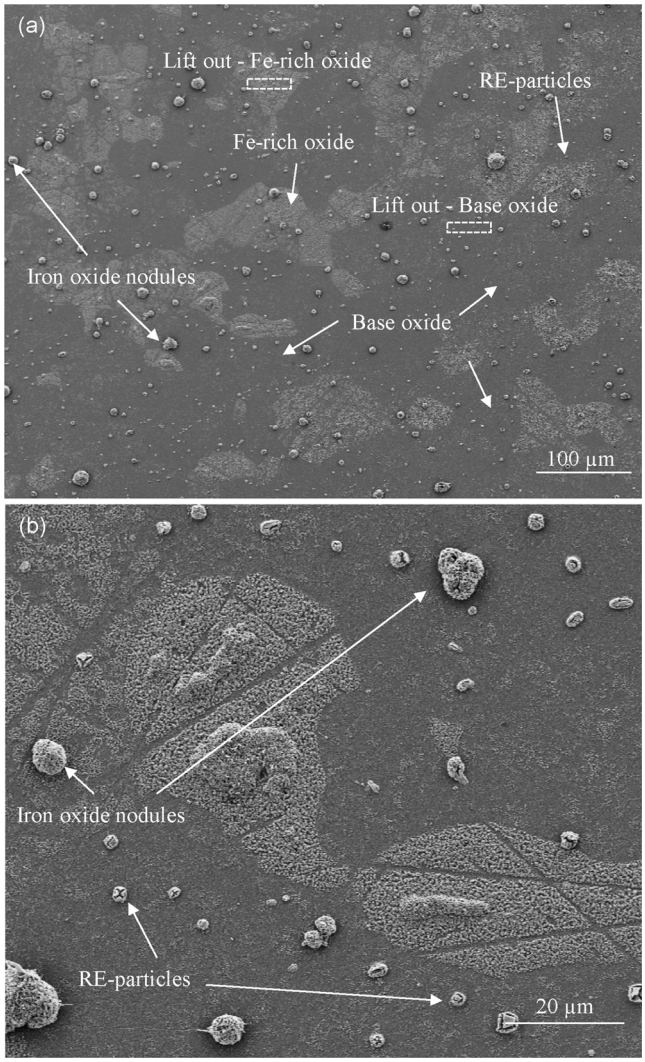

Fig. 3. (a–b) SEM-SE images at different magnifications of FeCrAl**0Si** after exposure in dry O_2 (5 % O_2 + N_2 (bal.)) at 600 °C for 168 h. Dashed rectangles in Fig. 3a marks two regions, Fe-rich oxide and base oxide, selected for further STEM analysis. Fig. 3b displays the key features of the surface morphology in higher magnification.

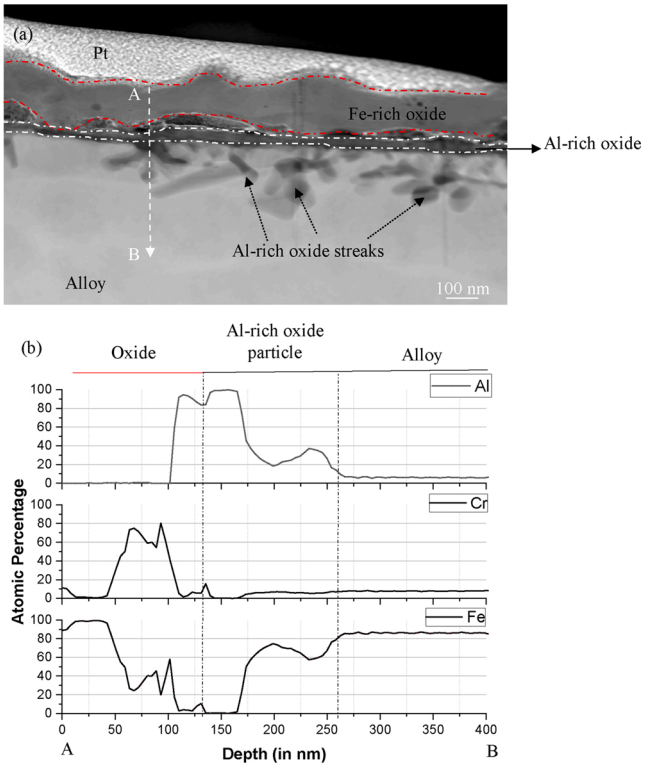

Fig. 4. (a) STEM/HAADF image of an Fe-rich oxide covered grain on FeCrAl**0Si** after exposure in dry O_2 (5 % O_2 + N_2 (bal.)) at 600 °C for 168 h. Fig. 4b displays the cationic concentrations from an EDS line scan performed along the dashed line from A to B shown in Fig. 4a.

found reaching into the bulk. A STEM/EDS line scan through the oxide into the alloy (A-B in Fig. 4b) verifies the presence of different layers observed in the HAADF image. The scale consists of an outer Fe-rich oxide layer of about 80−130 nm in thickness (bright contrast), followed by an Al-rich (roughly 100 at%) oxide layer with a thickness of about 50−75 nm (dark contrast). The STEM/EDS analysis of the dark contrast streaks underneath the Al-rich layer (indicated by dashed arrows in Fig. 4a) shows that they contain Al-rich oxide (60–75 at% Al, 10–15 % Cr and 25–40 at% Fe). However, due to the very small features, i.e. the thickness of the foil and the interaction volume during the analysis, it is hard to determine the exact composition.

Fig. 5a shows a STEM-HAADF image of a cross-section through the

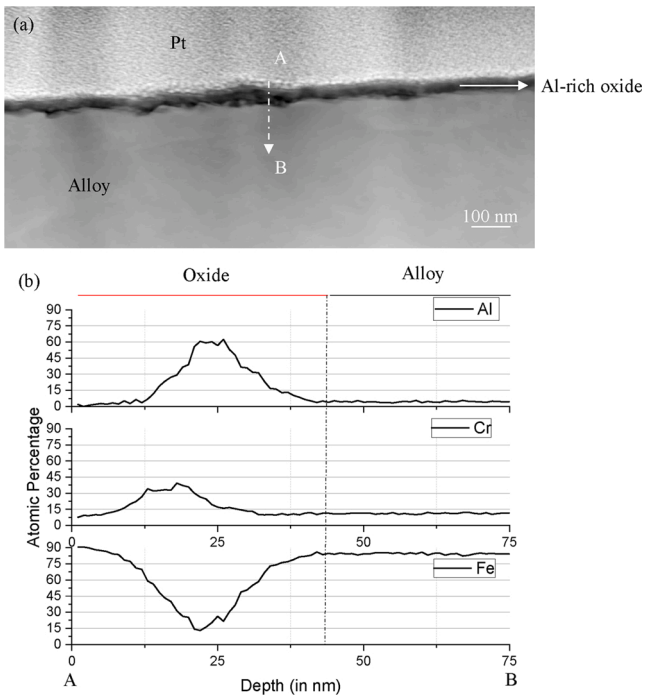

Fig. 5. (a) STEM/HAADF image showing the base oxide formed on FeCrAl**0Si** after exposure in dry O_2 (5 % O_2 + N_2 (bal.)) at 600 °C for 168 h. Fig. 5b displays the cationic concentrations from an EDS line scan performed along the dashed line from A to B shown in Fig. 5a.

base oxide on the FeCrAl**0Si** sample exposed at 600 °C in 5 %O_2 + N_2 (bal.) for 168 h. The image indicates a single layer with a more uniform thickness, around 40−75 nm. A representative STEM/EDS line scan is shown in Fig. 5b. The thin oxide scale has a layered structure. The 20 nm thick outer layer is Fe-rich (around 90 at%) followed by a 25 nm thick Cr-rich layer (30–40 at% Cr and equal amounts of Fe and Al). The 40 nm thick layer closest to the alloy is Al-rich (60–65 at%). It may be noted that there is a small Cr depleted zone in the alloy. It was not possible to determine the oxide grain size in any of the oxide layers as the oxide scale is very thin. However, HR-TEM analysis showed that all layers were crystalline.

3.2.2. *FeCrAl0Si – wet exposure*

All FeCrAl**0Si** samples displayed breakaway oxidation in the presence of water vapour. The microstructure of the oxide formed after breakaway has previously been shown to consist of a thick Fe-rich oxide [6] and is out of scope of this paper.

3.2.3. *FeCrAl2Si – dry exposure*

3.2.3.1. Oxide morphology. Fig. 6a-b displays SEM-SE images of the surface morphology of FeCrAl**2Si** after being exposed at 600 °C in 5 %O_2 + N_2 (bal.) for 168 h. The sample surface is covered by a base oxide and RE-particles protruding through it as can be seen in the higher magnification image (Fig. 6b). No iron oxide covered grains or iron oxide nodules can be observed. The morphology corresponds well with the calculated thickness. This is in good agreement with SEM/BSE imaging where the alloy grains were visible through the oxide (not shown here), indicating an oxide thickness in the nanometer range.

3.2.3.2. Oxide microstructure. The STEM image displayed in Fig. 7a shows a cross-section of the base oxide on the FeCrAl**2Si** sample after exposure at 600 °C in 5 %O_2 + N_2 (bal.) for 168 h. The oxide layer has a thickness of around 50 nm on all of the investigated regions. The results from a representative STEM/EDS line scan (Fig. 7b) shows that the scale is layered. It consists of a few nanometers thick outer Cr-rich layer (roughly 100 at%) followed by mixed Cr-Fe oxide phase. The two bottom layers are Al-rich, both of which consists of 40–75 at% Al. XRD analysis confirmed the presence of a corundum type oxide.

3.2.4. *FeCrAl2Si – wet exposure*

3.2.4.1. Oxide morphology. Fig. 8 shows an SEM-SE image of the surface morphology of the FeCrAl**2Si** sample after exposure at 600 °C in 5 %O_2 + 20 % H_2O + N_2(bal.) for 168 h. The sample's surface is covered by a base oxide and protruding RE-particles are evenly distributed on the surface as can be seen in the higher magnification image (Fig. 8b). No visible formation of iron oxide covered grains or presence of iron oxide nodules could be observed. The morphology corresponds well with a protective oxide scale (in the nanometer range) which corresponds well with the mass gain. This is further indicated by the alloy grains being visible through the thin oxide scale.

3.2.4.2. Oxide microstructure. The STEM-HAADF image displayed in Fig. 9 shows a cross-section of FeCrAl**2Si** after exposure at 600 °C in 5 % O_2 + 20 % H_2O + N_2(bal.) for 168 h. The oxide layer has a thickness of about 65 nm. A similar thickness was observed all over the sample in agreement with the SEM/BSE imaging. The results from a representative STEM/EDX line scan is shown in Fig. 9b. The outer part (~15 nm) of the scale is Si-rich (50–70 at% Si, 20–35 at% Al, 25 at% Fe and 0 at% Cr). The inner 50 nm part of the oxide scale is richer in Al with a composition of approximately 25–50 at% Al, 25–50 at% Fe, 5–10 at% Cr and Si 5–25

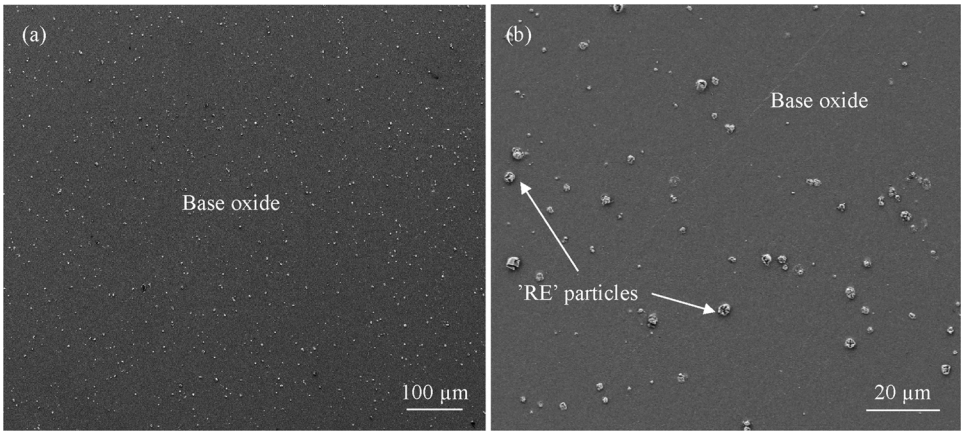

Fig. 6. (a–b) SEM-SE images at different magnifications of the FeCrAl**2Si** alloy after exposure in dry O_2 (5 % O_2 + N_2 (bal.)) at 600 °C for 168 h. Fig. 6b displays the key features in higher magnification.

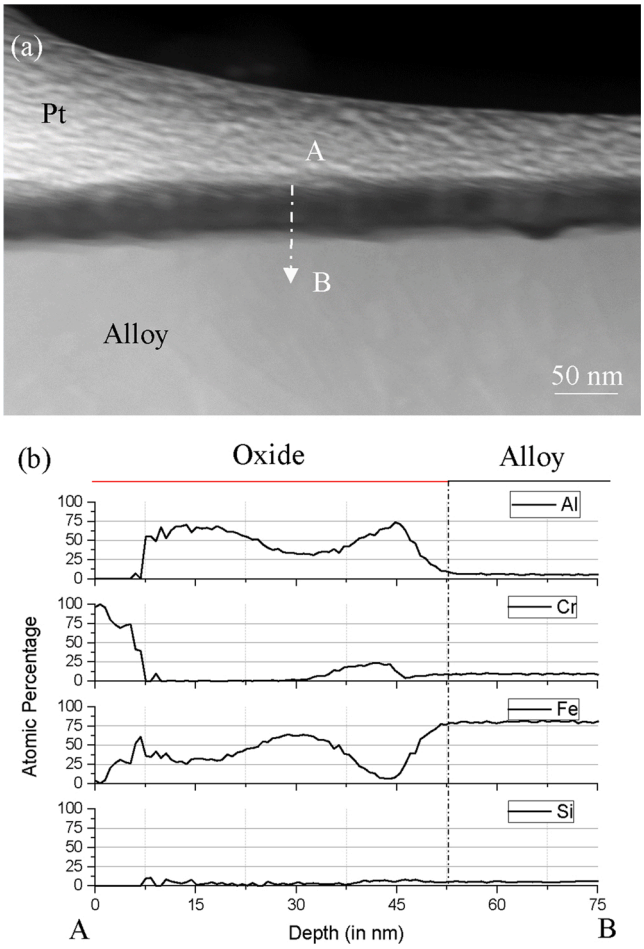

Fig. 7. (a) STEM/HAADF image showing the base oxide formed on FeCrAl**2Si** after exposure in dry O_2 (5 % O_2 + N_2 (bal.)) at 600 °C for 168 h. Fig. 7b displays the cationic concentrations from an EDS line scan performed on the dashed line from A to B shown in Fig. 7a.

at%. The oxide scale is thicker than the calculated thickness and in the same range as the base oxide formed on the FeCrAl**0Si** (dry) and FeCrAl**2Si** (dry).

3.3. Thermodynamic calculations

The additions of Si to the FeCrAl alloy may influence the properties of the oxide as well as the alloy. In order to investigate several aspects, thermodynamic calculations were performed. The interaction between Si and each of the key oxide forming elements, i.e. Al and Cr, were investigated by plotting the iso-activity lines for these elements in the alloy (BCC phase). The results are shown in Fig. 10, in which the iso-activity lines are projected on the corner of a pseudo-ternary isothermal section at 600 °C for the alloy containing Si

Fig. 10a shows the activity variation of Al in the alloy as a function of increased Si content. The red arrow shows that a higher Si-content intersect with an iso-activity line corresponding to a higher Al activity, i.e. addition of Si may increase the activity of Al in the alloy. The influence of Si on the Cr activity is shown in Fig. 10b. A higher Si content

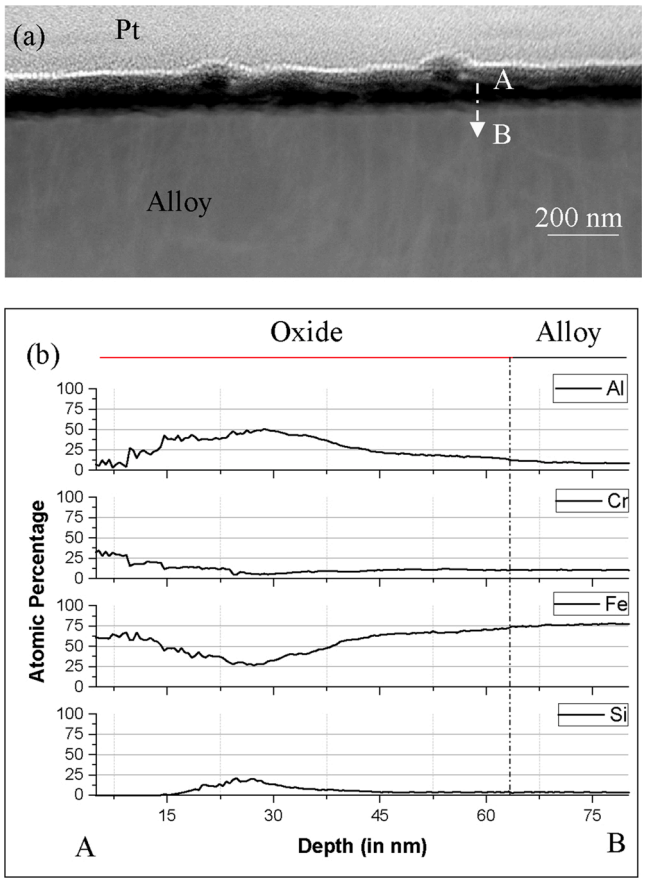

Fig. 9. (a) STEM/HAADF cross section image of the base oxide formed on FeCrAl**2Si** after exposure in wet O_2 (5 % O_2 + 20 % H_2O + N_2 (bal.)) at 600 °C for 168 h. Fig. 9b displays the cationic concentrations from an EDS line scan performed along the dashed line from A to B in Fig. 9a.

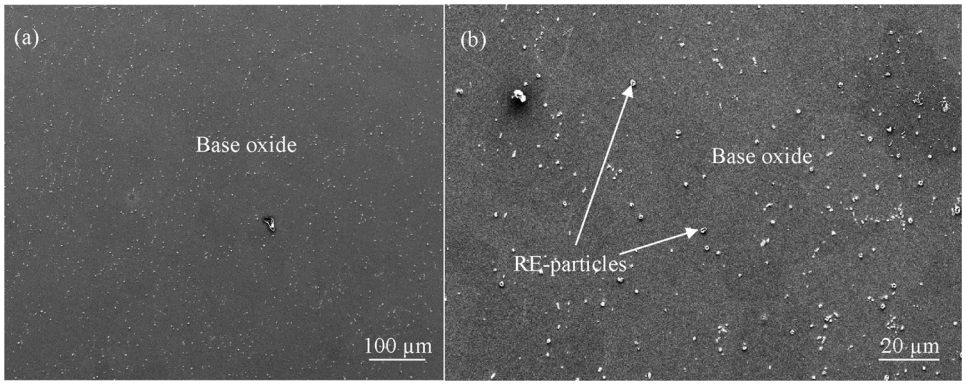

Fig. 8. (a–b) SEM-SE images at different magnifications of the FeCrAl**2Si** after exposure in wet O_2 (5 % O_2 + 20 % H_2O + N_2 (bal.)) at 600 °C for 168 h. Fig. 8b displays the key features in higher magnification.

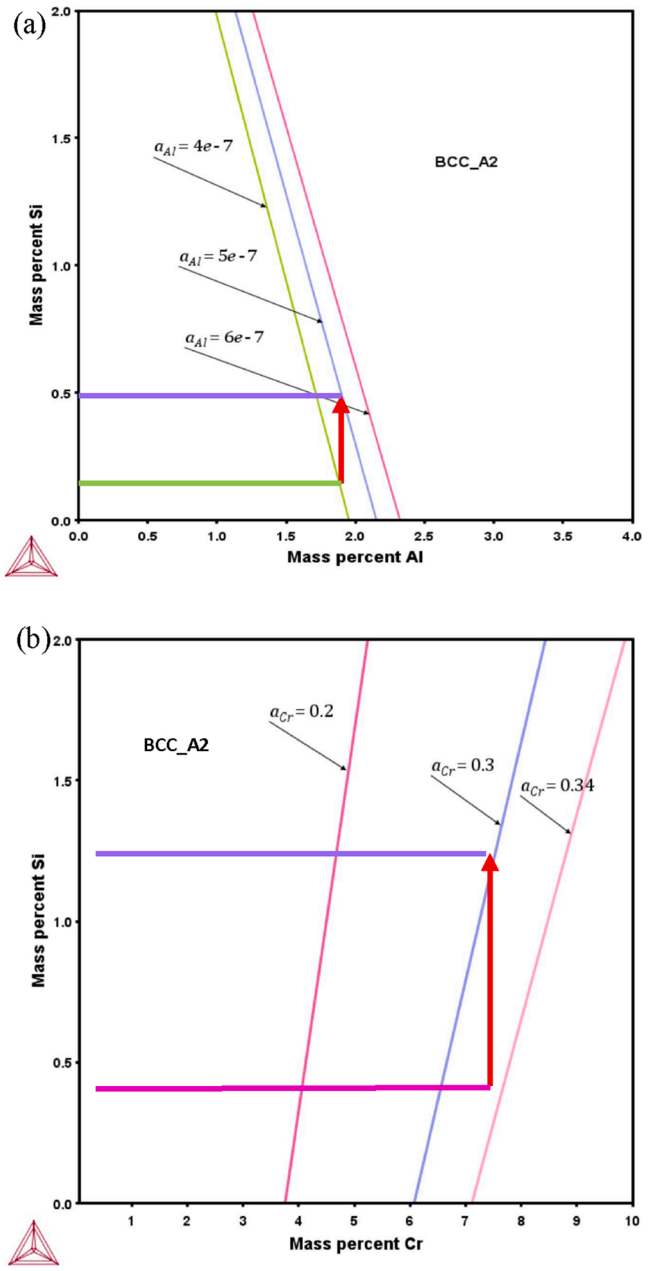

Fig. 10. The influence of Si-content in the alloy on the activity of a) Al and b) Cr in the alloy, attained by thermodynamic calculation using ThermoCalc.

(marked by the red arrow) intersects with a Cr iso-activity line representing a smaller value, i.e. addition of Si may decrease the activity of Cr in the alloy. Thus, these results indicate that the addition of Si to the alloy could result in a shift from a lower Al/Cr activity to a higher ratio, promoting a more Al-rich oxide scale. Similar calculations were performed for the oxide and a similar interaction was found between elements in the oxide (not shown). However, it was essential to include quartz in the calculations as it is an equilibrium product in the presence of Si. As no indications of quartz was found in our microstructural investigations, the oxide calculations do not reflect the present system and are not presented here.

The focus of the paper is on the thin protective oxide scales where the corundum phase is expected to be the dominant phase. Therefore, only the corundum phase was included in the thermodynamic oxide calculations. The protective properties of FeCrAl alloys is expected to depend on the Al_2O_3/Cr_2O_3-type of scale as was also observed in the microstructural investigation. The Al_2O_3/Cr_2O_3 oxide systems have a miscibility gap at 600 °C, see Fig. 11. The maximum allowed equilibrium Cr/Al ratio is 0.15 on the Cr-rich part of the $(Al,Cr)_2O_3$ scale while the maximum Al/Cr ratio is 6.8 on the Al-rich part of the $(Al,Cr)_2O_3$ scale.

The actual model alloys compositions were in addition used in order to predict the equilibrium composition of the oxide scale. The results from the calculations for FeCrAl**0Si** and FeCrAl**2Si** alloys are shown in Fig. 12. It should be noted that no Si is included in the corundum phase in the TCFE10 database. The calculations predict a layered scale in both cases with an Fe-rich outer scale and an Al-rich inner scale. Introducing Si indicates the formation of an Al-rich scale at a higher PO_2 as well as a Cr-rich middle part of the scale.

4. Discussion

The aim of the present paper is to investigate the influence of small additions of Si on the corrosion properties of FeCrAl alloys at 600 °C. The focus has been on the primary protection, i.e. the thin scale, and its properties. Careful exposures and thermodynamic calculations have been combined with detailed STEM-EDS analysis in order to link the microstructure to the behaviour of thin oxide scale formed under dry and wet oxidizing conditions.

4.1. General remarks

The gravimetric results (Fig. 1), show that the oxidation of the two model alloys can be described in terms of two distinct types of behaviour; (1) primary protection regime, i.e. protective oxide formation corresponding to a thin Al/Cr-rich corundum type oxide and a very low mass gain; (2) secondary protection, i.e. rapid oxidation corresponding to a poorly protective multilayer scale (average oxide thickness of about 80 μm). The exposure in dry O_2 at 600 °C resulted in the formation of a thin protective scale in both cases (FeCrAl**0Si** and FeCrAl**2Si**) while a thick, rapidly growing scale formed on FeCrAl**0Si** during exposure to wet O_2. This is in agreement with the results in a previous study where the addition of Si was shown to have an effect on the corrosion behaviour even after the breakaway oxidation on FeCrAl alloys [6]. However, the focus of this work is on the thin protective scale and the influence of Si on the microstructure in dry/wet environments.

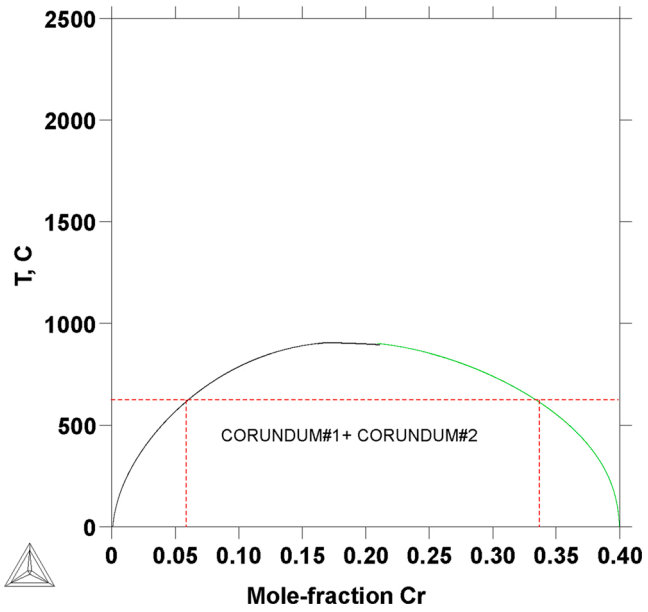

Fig. 11. The miscibility gap in the corundum phase (M_2O_3) in the Al-Cr-O system, attained by thermodynamical calculations using ThermoCalc.

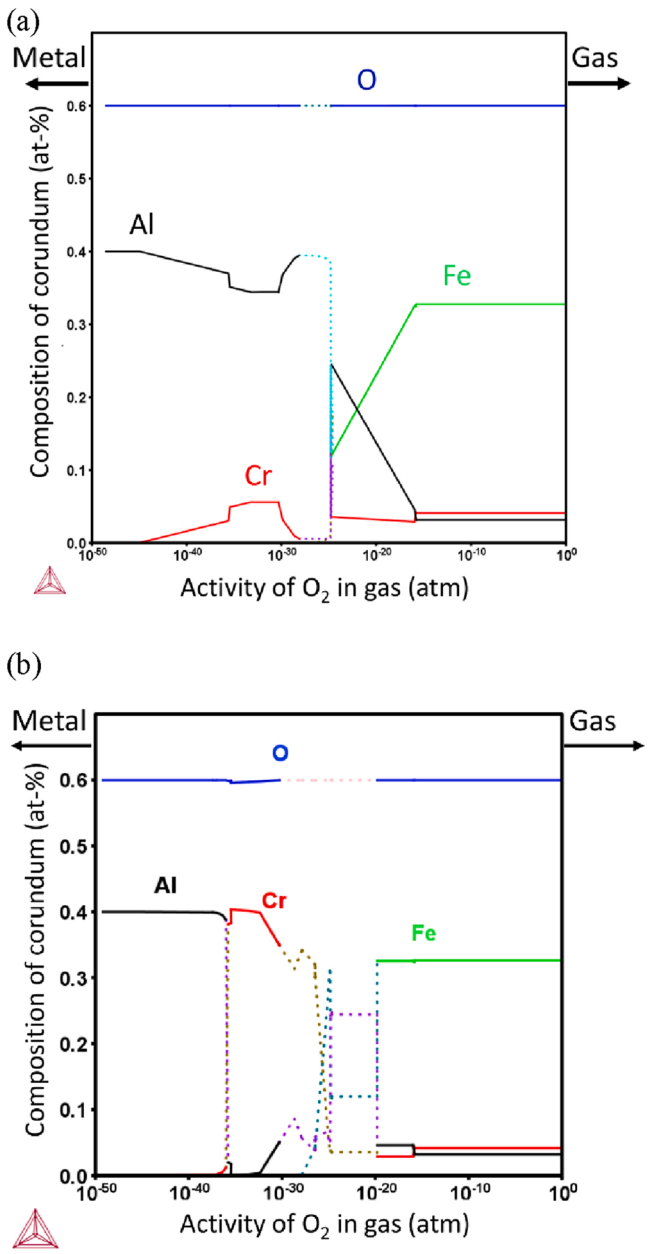

Fig. 12. Predicted equilibrium compositions of the corundum type oxide at different pO_2 for (a) FeCrAl**0Si** and (b) FeCrAl**2Si** attained by Thermodynamic calculations using ThermoCalc. The dotted lines show the compositions at values of pO_2 at which the corundum is metastable.

4.2. The thin protective scale - influence of Si

The morphology of the primary protection formed in the absence of Si (FeCrAl**0Si**) under dry conditions consist of three distinct features, i.e. iron oxide nodules (originating at RE-particles), alloy grains covered by Fe-rich oxide and a thin base oxide. The iron oxide nodules only cover a very small part of the surface and have not been investigated in detail in this work. However, in previous studies, a self-healing layer has been observed underneath the iron oxide covered RE-particles. The benefit of minor additions of RE to FeCrAl alloys has previously been shown to change the oxide growth mechanism as well as the transport processes within the oxide, resulting in reduced stresses within the oxide [23]. Thus, the adhesion of the protective oxide to the surface of the metal is greatly improved, which is crucial for the performance of FeCrAl alloys at elevated temperatures (above 800 °C), especially during thermal cycling. However, at lower temperatures (around 600 °C), this has been shown to not have a major impact on the adhesion of the protective oxide [19] which may be explained by the smaller thermal gradient when cooling down to room temperature. Mortazavi et al. investigated the interplay between water vapor and reactive elements (RE) at elevated temperatures (900−1000 °C) and found that the alumina-forming alloys enabled water to penetrate the oxide layer via hydroxylated and RE-ion decorated grain boundaries in the oxide [24]. However, at the lower temperature in the present study (600 °C), the relevance of this mechanism is not known.

The other distinct feature besides the dominating base oxide are the iron oxide covered grains. These do not seem to significantly increase with time (see Figs. 2 and 3) but the surface morphology of the oxide on these grains differs slightly after the 24 h and 168 h exposures. The protective behaviour of these regions may be explained by the Al-rich oxide layer formed at the metal/oxide interface, see Fig. 4. However, in addition to this, the microstructural investigation revealed indications of internal oxidation of Al below these regions. This microstructure (less protective grains) may, in a more corrosive environment (water vapor or alkali chlorides), act as initiation points for fast corrosion processes, causing breakaway oxidation and the formation of a multi-layered scale [25,26]. The reason for why some grains behaves differently is not fully understood but may be connected to the third element effect and the ability of each grain to form an initial chromia layer. The less protective grains may take longer time to form an initial chromia layer, which paves the way for iron oxide to form as an initial oxide layer instead, giving the Al enough time to form a protective oxide underneath. Comparing the Cr-content of the protective and less protective grains, it is significantly lower in the latter which may explain their inability to rapidly form a Cr-rich corundum type oxide. However, it is important to take into consideration that these model alloys are marginal chromia formers in comparison to commercial FeCrAl alloy which generally contain higher amounts of Cr.

The dominant morphology is the thin and protective oxide (base oxide in Fig. 5). It is single phase, consisting of a corundum-type solid solution. The STEM/EDS investigation of the base oxide shows that the Al/Cr-content in the oxide increases as the scale/metal interface is approached. This is in accordance with FeCr(Al) alloy oxidation, reported by Josefsson et al., and is a normal feature in the formation of protective scales on these alloys at lower temperatures (around 500 °C) [5]. In addition, the equilibrium calculations predict this composition, see Fig. 12. However, the measured composition is within the predicted miscibility gap of the $(Cr, Al)_2O_3$ oxide system, see Fig. 11, which means a segregation of a Cr-rich and an Al-rich phase. This is not in agreement with the STEM-EDS analysis or equilibrium calculations (Fig. 12). This may be explained by the relatively low temperature and thereby slow kinetics in the oxide scale which prolongs the time before equilibrium is achieved. An integration of the STEM/EDS line scans (Fig. 4 and more data not shown) indicates that the base oxide formed on the FeCrAl**0Si** alloy consists 23–33 at% of Al. None or very small depletion zones could be observed underneath the oxide.

Introducing Si in the alloy changes the surface morphology in dry oxygen as well as the resistivity of the protective oxide towards water vapour, which is discussed in the next section. The main differences between the oxide morphologies of FeCrAl**0Si** and FeCrAl**2Si** is the absence of Fe-rich oxide on the latter. Si-containing stainless steels have been shown to form a SiO_2 layer at the oxide/metal interface at elevated temperatures in similar environments (700−900 °C), resulting in improved corrosion behaviour. However, no enrichment of Si could be detected by the EDS analysis which means that no SiO_2 layer has formed (see Fig. 7). The equilibrium calculations may offer another explanation for the easier formation of a protective base oxide. The results from the calculations indicate that an increased Si-content in the alloy will increase the activity of Al and decrease the activity of Cr in the alloy, see Fig. 10. Since the activity of an element in an alloy increases if the concentration of that element is increased, the thermodynamic

calculations indicate that FeCrAl**2Si**, and Si-containing FeCrAl alloys in general, may behave as FeCrAl alloys with higher Al-content (which in general form more Al-rich oxides). The STEM/EDS results supports the calculations since the base oxide contains higher levels of Al for the Si-containing alloy than for the one without Si, compare Figs. 5 and 7. Integrating the Al-content of the thin base oxide of FeCrAl**2Si** (Fig. 7 and more data not shown) shows that it contains of 45–71 at% Al which is significantly higher compared to the base oxide corresponding to FeCrAl**0Si** (23–33 at% of Al). The increase in Al-content is in range with the increase observed when exposing a more highly alloyed FeCrAl alloy under the same conditions [5,7]. In addition, the STEM/EDS analysis indicates that the presence of Si results in most of the Cr being pushed out to the outer part of the oxide, leaving the rest of the oxide relatively free of Cr and more Al-rich. This may significantly affect the protectiveness of the corundum-type oxide. The thermodynamic calculations also show that pure alumina may be formed at higher pO_2 in the presence of Si, see Fig. 12. This may simplify the formation of an Al-rich oxide at an earlier stage of the oxidation process since the initial oxide (generally Cr-rich) does not need to reduce pO_2 as much before the Al-rich oxide can begin to form.

The theoretical calculations, based on the mass gain of FeCrAl**2Si** after exposure in 5 % O_2 + N_2 at 600 °C for 168 h, showed that the Cr_2O_3/Al_2O_3 thickness was 32−42 nm. Based on previous studies, a chromia layer grows faster than an alumina layer. Jonsson et al. [27] exposed a Fe-10Cr model alloy in dry oxygen at 600 °C for 168 h and found that the calculated chromia thickness was 90 nm, i.e. twice as thick as the oxide scale of FeCrAl**2Si** when exposed under these conditions. Josefsson et al. exposed a commercial FeCrAl alloy (Kanthal AF) in 5 % O_2 + N_2 at 600 °C for 168 h which resulted in a roughly 40 nm thick oxide [5]. The elevated presence of Al in the corundum type oxide results in a more protective scale even though it does not form a pure alumina.

4.3. The effect of water vapour in high pO_2 on FeCrAl alloys at 600 °C

The corrosivity of the combination of water vapour and O_2 towards stainless steel has been attributed to the vaporization of $CrO_2(OH)_2$ from the oxidizing metal surface [20,22,28]. Thus, it has been concluded that $(Fe_{1-x}Cr_x)_2O_3$ becomes less protective due to the resulting Cr depletion. This can trigger breakaway oxidation, i.e. the thin oxide being replaced by a thick scale consisting of hematite and spinel oxide (transitions from primary to secondary protection). The present investigation of FeCrAl model alloys supports this view since the very low calculated oxide thickness (smaller than the measured oxide thickness) indicates a mass loss. In addition, the vaporization of $CrO_2(OH)_2$ was confirmed by measuring the Cr-evaporation of the same alloys in a previous article [6]. Thus, the transformation of the thin protective oxide into a thick and poorly protective hematite/spinel scale in wet O_2 is preceded by a decrease in the concentration of Cr in the protective oxide. This may explain the rapid breakaway for FeCrAl**0Si** since the protective base oxide contains significant amounts of Cr. In contrary, the base oxide of FeCrAl**2Si** was shown to be significantly more Al-rich after exposure in dry conditions and may, according to the equilibrium calculations, form pure alumina at higher pO_2. This would explain the improved resistance of FeCrAl**2Si** to water vapour since a more Al-rich oxide is less vulnerable to Cr-evaporation. This is also in line with previous research on more highly alloyed FeCrAl alloys (with only trace amounts of Si) showing resistance towards water vapour (resists breakaway oxidation) under similar conditions [7,29]. The STEM-EDS analysis of FeCrAl**2Si** exposed in wet O_2, reported in Fig. 9b, shows that the outer part of the oxide is highly enriched in Si (50–70 at%) and displays an absence of Cr. Firstly, this indicates that Cr (which was enriched in the outer part of the oxide after exposure under dry conditions) is evaporated in the presence of water vapor, leaving behind a more protective oxide, on which the water vapor has little or no influence on further oxidation. Secondly, the STEM-EDS analysis shows a decreased Al-content throughout the oxide layers, compared to after exposure under dry conditions. Integrating the Al-content in the base oxide shows that it contains 24–30 at% Al which is in the same range as the base oxide formed on FeCrAl**0Si** under dry conditions. Yet, FeCrAl**2Si** displays significantly better corrosion resistance. It may be noted that the TEM lamellae of the FeCrAl**2Si** samples exposed under wet conditions are thicker than those from the samples exposed under dry conditions which may play a role in the quantification of the very thin Al-rich layer.

The local enrichment of Si in the oxide should be noted as it may have an influence on the corrosion resistance of the oxide formed on FeCrAl**2Si.** However, the mechanism is unclear and no conclusions regarding this can be drawn from the analysis performed in the present study. A possible explanation for the enrichment of Si at the outer part of the oxide is its proneness to react with water vapor to form SiO_2 [30,31]. SiO_2 may in turn react with Al_2O_3 to form an aluminosilicate, such as mullite [32,33]. A recent study on similar model alloys [34,35] also showed high enrichment of Si in the outer part of the oxide scale in after exposure under wet conditions. XRD analysis of the formed oxide indicated the presence of mullite. However, the exposure of that study was performed at 800 °C and may not be directly compared to the present study. No indications of mullite formation could be observed (XRD analysis) in the present study. However, the very thin oxide thickness may be the reason. In the possible case of mullite formation at the outer part of the oxide, this may influence the transport processes, such as reduced diffusivity of oxygen through the oxide. However, no literature on the diffusion properties of mullite in the present temperature range is available and thus, no comparison between the oxidation behavior of mullite and alumina can be made. The results in the present study does not indicate differences in transport processes since the oxide thickness on FeCrAl**2Si** after exposure under dry (no Si present in oxide) and wet (Si present in oxide) conditions is in the same range. Regardless of the origin of the enrichment of Si in the oxide scale, the decreased amount of Cr in the oxide scale, reducing the sensitivity towards Cr-evaporation, is a possible reason for the increased corrosion resistance.

5. Conclusions

- Minor additions of Si to a FeCrAl model alloy increases the protectiveness of the thin base oxide at 600 °C
- Dry O_2:
  - More rapid formation of protective base oxide
  - More Al-rich oxide
    - In agreement with thermodynamic calculations showing increased activity of Al and decreased activity of Cr in presence of Si in the alloy
- Wet O_2:
  - Resistance towards breakdown upon addition of Si
  - Possible explanations:
    - More Al-rich oxide
    - Si-enrichment in the outer part of the oxide scale
    - Significantly reduced Cr-content in oxide scale

Author's contribution statement

Vijayshankar Asokan carried out analysis on scanning electron microscopy and transmission electron microscopy, written results and discussions based on the images and EDS data.

Johan Eklund carried out corrosion experiments and derived corrosion mechanism theories from the available data related to the present paper and written major part of the discussions together with Torbjörn Jonsson.

Sedi Bigdeli carried out thermodynamic calculations using Thermo-Calc software and provided reports related to the experiments and helped out in discussion.

Torbjörn Jonsson involved in preliminary design of the experiments both in corrosion exposures and in microscopy analysis. He also

involved in the discussion with Sedi to co-ordinate the theoretical understanding to the experimental section. He also involved in discussion with Vijayshankar Asokan and Johan Eklund throughout the construction of this manuscript.

Data availability

The raw/processed data required to reproduce these findings cannot be shared at this time due to technical or time limitations.

Declaration of Competing Interest

The authors report no declarations of interest.

Acknowledgements

This work was carried out within the Swedish High Temperature Corrosion Center (HTC). The authors are grateful to Kanthal for supporting and supplying materials for this study. The microscopic investigation was carried out at Chalmers Materials Analysis Laboratory (CMAL).

References

[1] P. Kofstad, High Temperature Corrosion, Elsevier Applied Science Publishers, Crown House, Linton Road, Barking, Essex IG 11 8 JU, UK, 1988, 1988.
[2] H. Götlind, F. Liu, J.E. Svensson, M. Halvarsson, L.G. Johansson, The effect of water vapor on the initial stages of oxidation of the FeCrAl alloy kanthal AF at 900 °C, Oxid. Met. 67 (5) (2007) 251–266.
[3] F. Liu, H. Josefsson, J.-E. Svensson, L.-G. Johansson, M. Halvarsson, TEM investigation of the oxide scales formed on a FeCrAlRE alloy (Kanthal AF) at 900°C in dry O2 and O2 with 40% H2O, Mater. High Temp. 22 (3–4) (2005) 521–526.
[4] D.J. Young, High Temperature Oxidation and Corrosion of Metals, Elsevier, 2008.
[5] H. Josefsson, F. Liu, J.E. Svensson, M. Halvarsson, L.G. Johansson, Oxidation of FeCrAl alloys at 500–900°C in dry O2, Mater. Corros. 56 (11) (2005) 801–805.
[6] J. Eklund, B. Jönsson, A. Persdotter, J. Liske, J.E. Svensson, T. Jonsson, The influence of silicon on the corrosion properties of FeCrAl model alloys in oxidizing environments at 600 °C, Corros. Sci. 144 (2018) 266–276.
[7] N. Israelsson, J. Engkvist, K. Hellström, M. Halvarsson, J.-E. Svensson, L.-G. Johansson, KCl-induced corrosion of an FeCrAl alloy at 600 °C in O2 + H2O environment: the effect of pre-oxidation, Oxid. Met. 83 (1) (2015) 29–53.
[8] T.D. Nguyen, J. Zhang, D.J. Young, Effects of Silicon on high temperature corrosion of Fe–Cr and Fe–Cr–Ni alloys in carbon dioxide, Oxid. Met. 81 (5) (2014) 549–574.
[9] Y. Wouters, G. Bamba, A. Galerie, M. Mermoux, J.-P. Petit, Oxygen and water vapour oxidation of 15Cr ferritic stainless steels with different silicon contents, Mater. Sci. Forum 461–464 (2004) 839–848.
[10] T.D. Nguyen, J. Zhang, D.J. Young, Effects of silicon and water vapour on corrosion of Fe–20Cr and Fe–20Cr–20Ni alloys in CO2 at 650 °C, Oxid. Met. 87 (3) (2017) 541–573.
[11] T. Jonsson, S. Canovic, F. Liu, H. Asteman, J.E. Svensson, L.G. Johansson, et al., Microstructural investigation of the effect of water vapour on the oxidation of alloy 353 MA in oxygen at 700 and 900°C, Mater. High Temp. 22 (3–4) (2005) 231–243.
[12] T. Jonsson, F. Liu, S. Canovic, H. Asteman, J.-E. Svensson, L.-G. Johansson, et al., Influence of H[sub 2]O(g) on the Oxide Microstructure of the Stainless Steel 353MA at 900°C in Oxygen, 2007.
[13] S. Kiamehr, K.V. Dahl, M. Montgomery, M.A.J. Somers, KCl-induced high temperature corrosion of selected commercial alloys, Mater. Corros. 67 (1) (2016) 26–38.
[14] F. Velasco, A. Bautista, A. González-Centeno, High-temperature oxidation and aqueous corrosion performance of ferritic, vacuum-sintered stainless steels prealloyed with Si, Corros. Sci. 51 (1) (2009) 21–27.
[15] J. Dunning, D. Alman, J.J.O.o.M. Rawers, Influence of silicon and aluminum additions on the oxidation resistance of a lean-chromium stainless steel, Oxid. Met. 57 (5–6) (2002) 409–425.
[16] R. Pettersson, L. Liu, J.J.C.e. Sund, Cyclic oxidation performance of silicon-alloyed stainless steels in dry and moist air, Corros. Eng. Sci. Technol. 40 (3) (2005) 211–216.
[17] T. Oshima, Y. Habara, K. Kuroda, Effects of si on oxidation behaviors in Cr-Mn-Ni austenitic stainless steels, Mater. Sci. Forum 539 (2007) 4897–4902. Trans Tech Publ.
[18] L. Mikkelsen, S. Linderoth, J. Bilde-Sørensen, The effect of silicon addition on the high temperature oxidation of a Fe-Cr alloy, Mater. Sci. Forum 461 (2004) 117–122. Trans Tech Publ.
[19] A. Persdotter, J. Eklund, J. Liske, T. Jonsson, Beyond breakaway corrosion - Influence of Cr, Ni and Al on corrosion of Fe-based alloys at 600 °C, Corros. Sci. (2020). Accepted.
[20] H. Asteman, K. Segerdahl, J.E. Svensson, L.G. Johansson, M. Halvarsson, J.E. Tang, et al., Oxidation of stainless steel in H2O/O-2 environments - role of chromium evaporation, in: P. Steinmetz, I.G. Wright, G. Meier, A. Galerie, B. Pieraggi, R. Podor (Eds.), High Temperature Corrosion and Protection of Materials 6, Prt 1 and 2, Proceedings, Trans Tech Publications Ltd, Zurich-Uetikon, 2004, pp. 775–782.
[21] J. Engkvist, S. Canovic, F. Liu, H. Götlind, J.E. Svensson, L.G. Johansson, et al., Oxidation of FeCrAl foils at 500–900°C in dry O2 and O2 with 40% H2O, Mater. High Temp. 26 (2) (2009) 199–210.
[22] H. Asteman, J.E. Svensson, L.G. Johansson, M. Norell, Indication of chromium oxide hydroxide evaporation during oxidation of 304L at 873 K in the presence of 10% water vapor, Oxid. Met. 52 (1) (1999) 95–111.
[23] D.P. Whittle, J. Stringer, Improvements in high temperature oxidation resistance by additions of reactive elements or oxide dispersions, Philos. Trans. R. Soc. Lond. Ser. A, Math. Phys. Sci. 295 (1413) (1980) 309–329.
[24] N. Mortazavi, C. Geers, M. Esmaily, V. Babic, M. Sattari, K. Lindgren, et al., Interplay of water and reactive elements in oxidation of alumina-forming alloys, Nat. Mater. 17 (7) (2018) 610–617.
[25] T. Jonsson, H. Larsson, S. Karlsson, H. Hooshyar, M. Sattari, J. Liske, et al., High-temperature oxidation of FeCr(Ni) alloys: the behaviour after breakaway, Oxid. Met. 87 (3–4) (2017) 333–341.
[26] T. Jonsson, S. Karlsson, H. Hooshyar, M. Sattari, J. Liske, J.E. Svensson, et al., Oxidation after breakdown of the chromium-rich scale on stainless steels at high temperature: internal oxidation, Oxid. Met. 85 (5) (2016) 509–536.
[27] T. Jonsson, B. Pujilaksono, H. Heidari, F. Liu, J.E. Svensson, M. Halvarsson, et al., Oxidation of Fe–10Cr in O2 and in O2+H2O environment at 600°C: a microstructural investigation, Corros. Sci. 75 (2013) 326–336.
[28] H. Asteman, J.E. Svensson, L.G. Johansson, Evidence for chromium evaporation influencing the oxidation of 304L: the effect of temperature and flow rate, Oxid. Met. 57 (3) (2002) 193–216.
[29] N. Israelsson, K. Hellström, J.-E. Svensson, L.-G. Johansson, KCl-induced corrosion of the FeCrAl alloy kanthal ® AF at 600 °C and the effect of H2O, Oxid. Met. 83 (1) (2015) 1–27.
[30] C.-H. Lin, Oxidation (of silicon), in: D. Li (Ed.), Encyclopedia of Microfluidics and Nanofluidics, Springer US, Boston, MA, 2008, p. 1584.
[31] D.R. Wolters, On the oxidation kinetics of silicon: the role of water, J. Electrochem. Soc. 127 (9) (1980) 2072–2082.
[32] H. Schneider, J. Schreuer, B. Hildmann, Structure and properties of mullite—a review, J. Eur. Ceram. Soc. 28 (2) (2008) 329–344.
[33] H. Schneider, R.X. Fischer, J. Schreuer, Mullite: crystal structure and related properties, J. Am. Ceram. Soc. 98 (10) (2015) 2948–2967.
[34] T. Sand, A. Edgren, C. Geers, V. Asokan, J. Eklund, T. Helander, et al., Exploring the silicon effect on the high temperature corrosion behaviour of FeCrAl alloys in humid air, Submitted to Oxidation of Metals, Oxid. Met. (2020).
[35] A. Edgren, High Temperature Corrosion of FeCrAl Alloys in Humidified Environment, Department of Chemistry and Chemical Engineering. Chalmers University of Technology, 2019.